Supplement of Atmos. Chem. Phys., 26, 13157–13173, 2026
https://doi.org/10.5194/acp-26-13157-2026-supplement

Supplement of

An observational perspective on precipitation efficiency of mesoscale convective systems over the Asian Monsoon Region

Thabo Makgoale et al.

Correspondence to: Thabo Makgoale (temakgoale@arizona.edu) and Sylvia Sullivan (sylvia@arizona.edu)

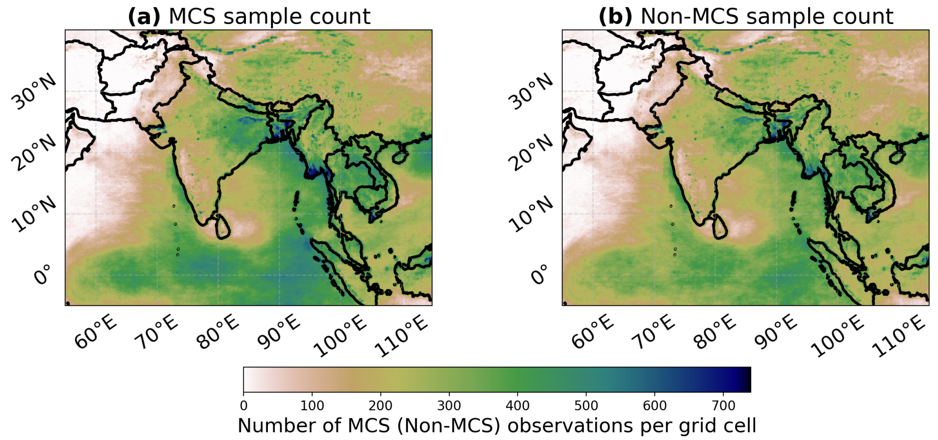

Figure S1. *Regions with larger sample counts indicate locations where ε estimates are based on more observations.* Spatial distribution of sample sizes at each 0.1° grid cell for (a) MCS and (b) non-MCS ε calculations over the Asian monsoon region during 10 August–10 September 2016.

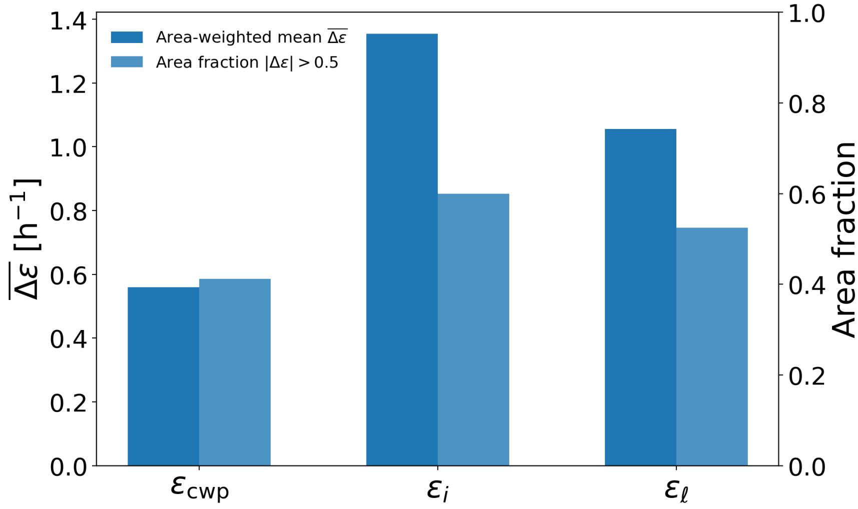

Figure S2. *Ice-phase efficiency (ε_i) exhibits both a larger domain-mean enhancement and broader spatial coverage than ε_ℓ.* Bars chart show the area-weighted mean difference $\overline{\Delta\varepsilon} = \varepsilon_{\mathrm{MCS}} - \varepsilon_{\mathrm{nonMCS}}$ (left axis) and the fractional spatial coverage where the magnitude of the difference exceeds a physically meaningful threshold ($|\Delta\varepsilon| > \tau$, right axis) for cloud water path efficiency ($\varepsilon_{\mathrm{cwp}}$), ice-phase efficiency (ε_i), and liquid-phase efficiency (ε_ℓ). Area weighting is applied using $\cos(\phi)$.

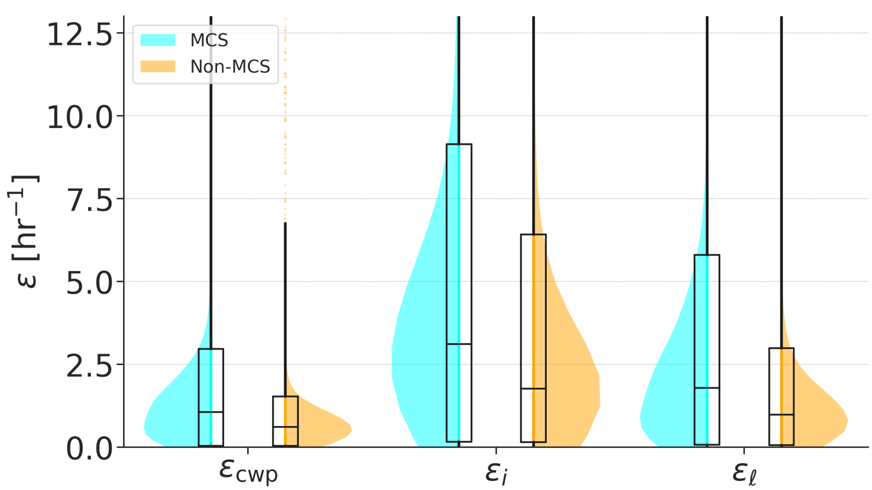

Figure S3. *MCSs have substantially higher ε across all phases, with median ε values roughly double those of non-MCS convection.* For readability, only one half of each violin distribution is displayed; this half-violin style prevents overlap between MCS (cyan) and non-MCS (orange) distributions. From left to right, box plots show overall total precipitation efficiency (ε_{cwp}), ice-phase precipitation efficiency (ε_i), and liquid-phase precipitation efficiency (ε_ℓ). The boxes indicate the interquartile range, the horizontal line marks the median, and the violin width denotes data density. Whiskers extend to the 5st and 95th percentiles.

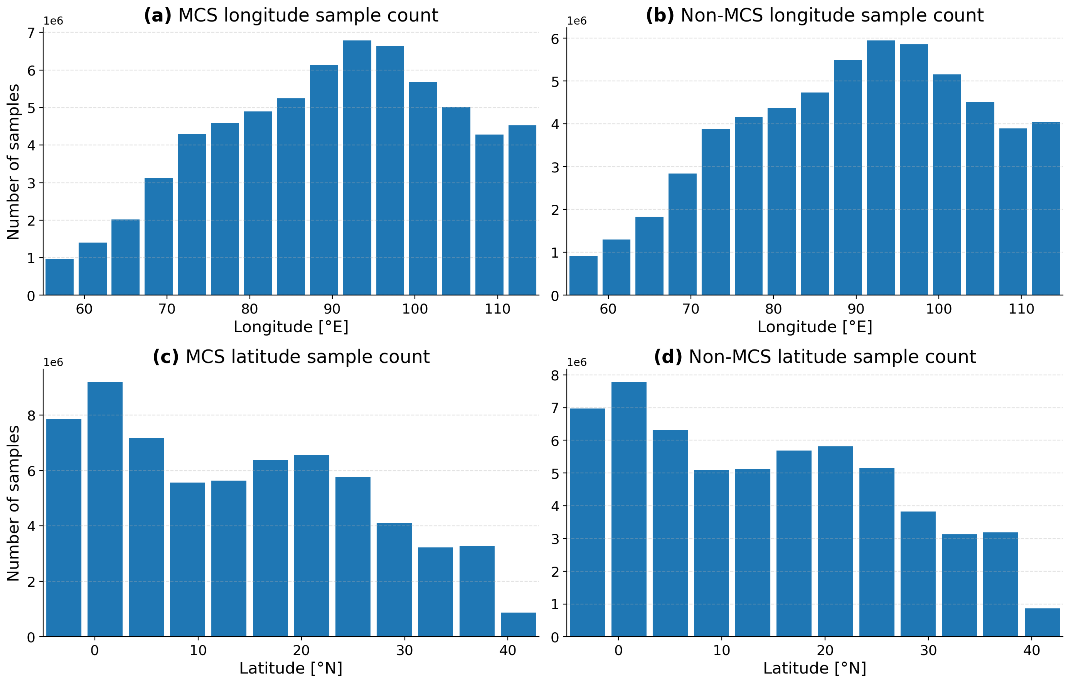

Figure S4. *Each longitude and latitude bin contains $\mathcal{O}(10^6)$ samples of MCS versus non-MCS.* Bar plots showing the sample size contributing to each spatial bin used to calculate the median ε in Figure. 4. Panels (a) and (b) show the sample counts for the longitudinal bins for MCS and non-MCS conditions, respectively, while panels (c) and (d) show the corresponding sample counts for the latitudinal bins. Sample counts represent the total number of valid grid-cell observations included within each longitude or latitude bin over the full analysis period (10 August–10 September 2016).

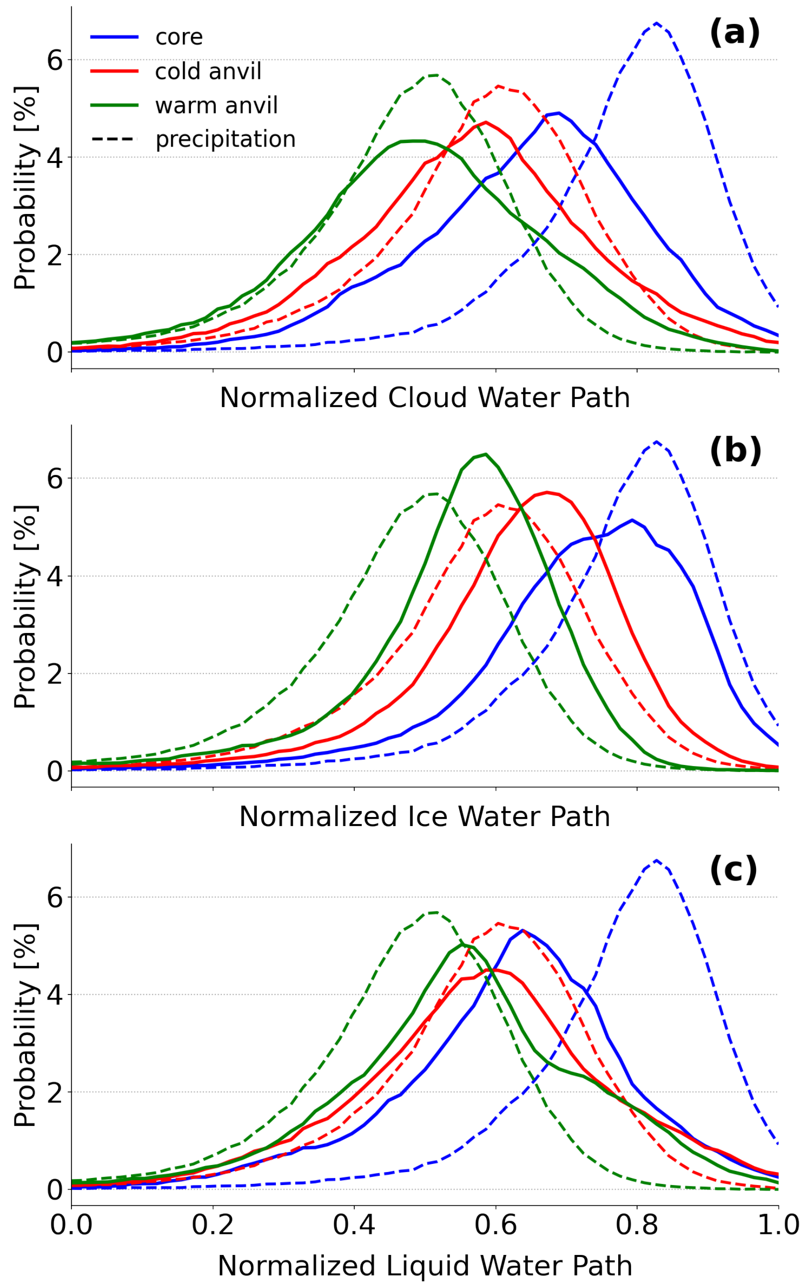

Figure S5. *Precipitation is systematically shifted toward higher normalized values than condensate within core of MCS for all three condensate metrics.* Normalized probability distributions comparing column-integrated cloud condensate (solid lines) and precipitation (dashed lines) across three MCS sub-regions over the Asian monsoon domain for 10 Aug–10 Sep 2016. Panels show (a) cloud water path (CWP), (b) ice water path (IWP), and (c) liquid water path (LWP) for the convective core (blue), cold anvil (red), and warm anvil (green). For each variable, distributions are computed from all valid grid cells after removing missing values and are expressed as probability (%). The horizontal axis is a 0–1 normalized coordinate obtained by log-transforming bin centers and scaling to the range of each variable.

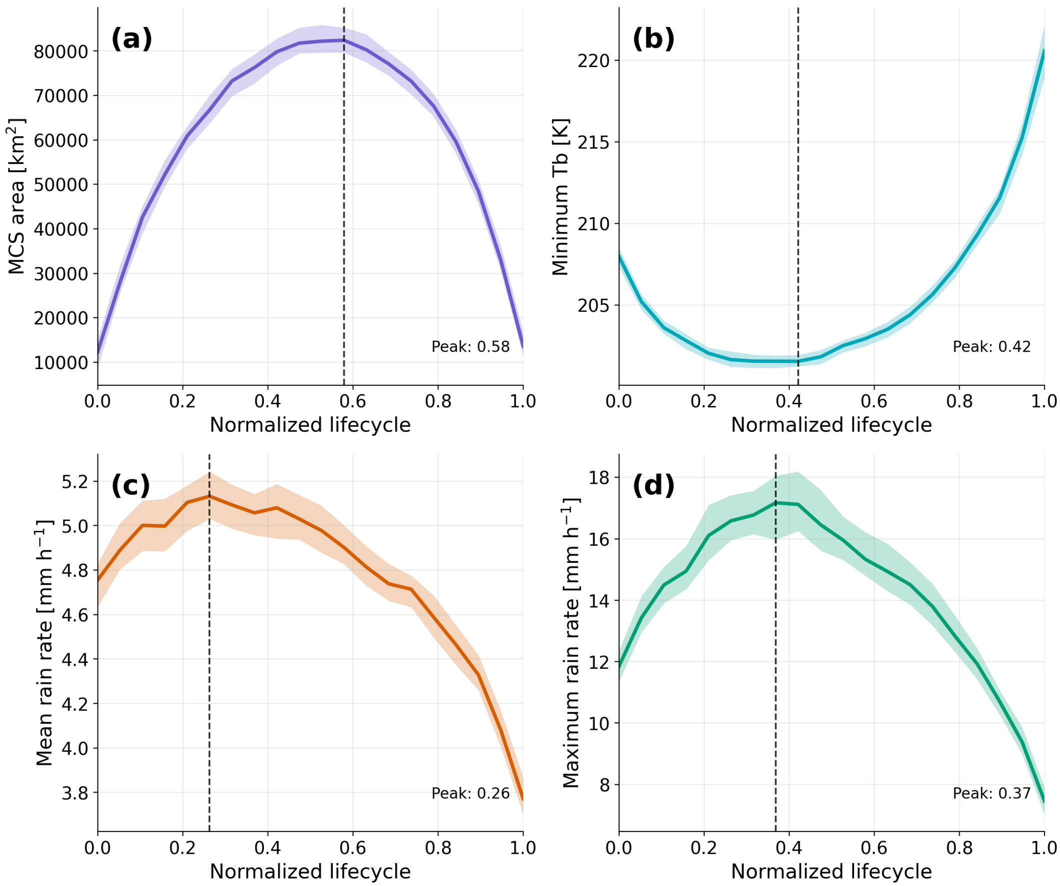

Figure S6. *MCSs reach peak convective intensity before maximum spatial extent.* Normalized lifecycles of (a) MCS area, (b) minimum cloud-top brightness temperature (Tb), (c) mean rain rate, and (d) maximum rain rate for all MCSs in the study domain. Individual MCS lifetimes were normalized to a common 0–1 lifecycle coordinate, where 0 and 1 correspond to initiation and dissipation, respectively, and interpolated onto common lifecycle bins before compositing. Solid lines show the median value across all systems, while shading indicates the 95% bootstrap confidence interval. Vertical dashed lines denote the lifecycle stage at which the median reaches its maximum (area and rain-rate metrics) or minimum (Tb).

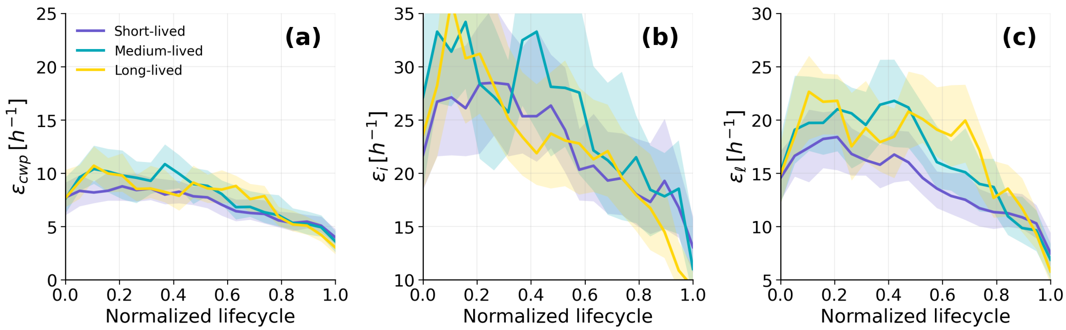

Figure S7. *Differences between lifetime categories are relatively modest for total precipitation efficiency ($\varepsilon_{\mathrm{cwp}}$), whereas ε_i and ε_ℓ show much larger separation, indicating that condensate partitioning and microphysical processes are more sensitive to storm longevity.*Normalized lifecycle evolution of (a) ($\varepsilon_{\mathrm{cwp}}$), (b) ($\varepsilon_i$), and (c) ($\varepsilon_\ell$) for short-lived (4–8 h), medium-lived (8–12 h), and long-lived (>12 h) MCSs. Each MCS lifecycle was normalized to a common 0–1 coordinate and interpolated onto common lifecycle bins before compositing. Solid lines denote the median, and shading indicates the 95% bootstrap confidence interval

Table C1. Pearson correlation coefficients (r) and associated p-values for the relationship between precipitation efficiency ($\varepsilon_{\rm cwp}$, ε_{ℓ}, ε_i) and MCS area, stratified by microphysical phase, for both mean rain rate and maximum rain rate. All correlations are statistically significant at the 95% confidence level (p $<$ 0.05).

Rain-rate metric	**Efficiency component**	r	p**-value**
Mean	$\varepsilon_{\rm cwp}$	0.9835	1.11×10^{-5}
	ε_{ℓ}	0.9847	8.84×10^{-6}
	ε_i	0.9789	2.32×10^{-5}
Max	$\varepsilon_{\rm cwp}$	0.9512	2.81×10^{-4}
	ε_{ℓ}	0.9539	2.36×10^{-4}
	ε_i	0.9467	3.63×10^{-4}

Table C2. Pearson correlation coefficients (r) and associated p-values for the relationship between precipitation efficiency ($\varepsilon_{\rm cwp}$, ε_{ℓ}, ε_i) and brightness temperature (Tb), stratified by microphysical pathway and rain-rate metric. Results are shown separately for mean and maximum rain rates. All correlations are statistically significant at the 95% confidence level ($p < 0.05$).

Rain-rate metric	**Efficiency component**	r	p**-value**
Mean	$\varepsilon_{\rm cwp}$	-0.9752	3.74×10^{-5}
	ε_{ℓ}	-0.9786	2.41×10^{-5}
	ε_i	-0.9880	4.27×10^{-6}
Max	$\varepsilon_{\rm cwp}$	-0.9930	8.68×10^{-7}
	ε_{ℓ}	-0.9894	2.95×10^{-6}
	ε_i	-0.9921	1.21×10^{-6}